Supporting Information

Black/red phosphorus quantum dots for photocatalytic water splitting: From type I heterostructure to Z-Scheme system

Rui Shi,[a] Fulai Liu,[a,c] Zhuan Wang,[b] Yuxiang Weng,[b,c] Yong Chen*[a,c]

a Key Laboratory of Photochemical Conversion and Optoelectronic Materials & HKU-CAS Joint Laboratory on New Materials, Technical Institute of Physics and Chemistry, Chinese Academy of Sciences, Beijing 100190, People's Republic of China

b Bejing National Laboratory for Condensed Matter Physics & CAS Key Laboratory of Soft Matter Physcis, Institute of Physics, Chinese Academy of Sciences, Beijing 100190, People's Republic of China

c University of Chinese Academy of Sciences, Beijing 100049, People's Republic of China

Materials

All materials were of analytical grade and used as received without further purification. Red phosphorus, ethylenediamine, 1-methyl-2-pyrrolidinone (NMP) were obtained from Sinopharm Chemcial Reagent Co., Ltd (Shanghai, China).

Preparation of samples

Black phosphorus/red phosphorus heterostructure (BP/RP) was prepared in ethylenediamine under refluxing condition. Briefly, 500 mg RP and 80 mL ethylenediamine solution were mixed together. Then the mixtures were refluxed at 120 ^{o}C on a mantle heater for 6 h. The as-prepared BP/RP heterostructure was collected by centrifugation, washed with deionized water and ethanol for three times, dried in air for 12 h.

BP/RP-QD was prepared by adding 50 mg BP/RP into 20 mL deionized water, which was sonicated to form a homogeneous dispersion. Then the dispersion was centrifuged for 10 min at a speed of 6000 rpm. The obtained supernatant contained BP/RP-QD.

BP-QD was synthesized according to the reported method.[S1] RP-QD was fabricated in NMP solvent under ultrasonication condition. Briefly, 30 mg of bulk red phosphorus was added into 30 mL NMP solvent. The dispersion was sonicated for 20 h by using an ultrasonic cleaner at 70 W output power. The resultant dispersion was centrifuged for 10 min at a speed of 8000 rpm. The obtained supernatant contained RP-QD.

Photocatalytic activity measurement

Photocatalytic water splitting experiments were carried out in 20 mL quartz tube sealed with silicone rubber septum. 1 mg photocatalyst and 5 mL water were added into the tube. In order to further improve the photocatalytic performance, a certain amount of $Co(NO_3)_2$ was added to the above suspension. Cobalt ions could be deposited on the surface of photocatalyst to act as co-catalyst to promote photocatalytic activity. Then, the system was deoxygenated with Ar for 30 min to remove the air before irradiation. A LED light (12 W, λ=420 ± 10 nm) was used as the irradiation light source. The LED was positioned 1 cm away from the sample

which was kept under continuously stirring at room temperature. The quantities of H_2 evolution were measured by a gas chromatograph (GC-2014C, Shimadzu, with Ar as carrier gas), which was equipped with a 5 Å molecular sieve column (3 m × 2 mm) and a thermal-conductivity detector. The number of incident photons was 1.05×10^{17} photons s^{-1} which was measured using an irradiance meter. The apparent quantum efficiency (AQE) was calculated according to the equation below:

$$AQE = \frac{number\ of\ reacted\ electrons}{number\ of\ incident\ photons} \times 100\%$$
$$= \frac{number\ of\ evolved\ H_2\ molecules \times 2}{number\ of\ incident\ photons} \times 100\%$$

The PL measurements of hydroxyl radical were as follows: 1 mg sample was suspended in 5 mL aqueous solution containing 10 mM NaOH and 3 mM terephthalic acid. Before exposure to visible-light irradiation, suspension was deoxygenated with Ar for 30 min and stirred in the dark for 30 min. Then the solution was taken out and centrifuged for PL measurements. The content of PO_x^{3-} produced from sample during the photocatalytic water splitting was measured by ion chromatography. Ion chromatography analysis was performed using Metrohm-761 Compact with an IonPac AS19 RFIC analytical column. The experiments were carried with 30 mM KOH as eluent and column temperature was 30 ^oC.

Materials characterization

The purity and crystallinity of the as-prepared sample were characterized by XRD on a Bruker D8-advance diffractometer using Cu Kα (λ=1.54056 Å). The XRD data for indexing and cell-parameter calculation were collected in a scanning mode with a step length of 0.1^o and a preset time of 1s/step. Morphologies and structure of the as-prepared sample were examined with high resolution transmission electron microscopy (HRTEM) by JEM 2100F field emission gun transmission electron microscope operated at an accelerating voltage of 200 kV. Diffuse reflection spectra (DRS) were obtained on a Varian-Cary 5000 UV-Vis-IR spectrophotometer. Raman measurements were obtained using a Renishaw inVia-Reflex spectrometer equipped with a notch filter and a CCD detector. Chemical characterization of the sample surface was performed with X-ray photoelectron spectroscopy (XPS ThermoFisher

ESCALAB 250Xi). The charge effect was calibrated using the binding energy of C1s. UV photoelectron spectroscopy (UPS) data were collected with a homemade He lamp source which produces a resonance line He Ⅰ (21.2 eV). The in-situ electron paramagnetic resonance (EPR) measurement was carried out using an Endor spectrometer (Bruker E500) at room temperature. The g factor was obtained by taking the signal of manganese as standard. The EPR spectrometer was coupled to a computer for data acquisition and instrument control. The magnetic parameters of the radicals detected were obtained from direct measurements of the magnetic field and microwave frequency. Steady-state photoluminescence (PL) spectra of the sample were investigated utilizing the Edinburgh Instruments-FLS 1000. Thermogravimetric analysis (TGA) was executed via a Diamond TG/DTA simultaneous thermal analyzer. The time-resolved transient absorption spectra (TAS) measurements were prepared as the following procedure: The laser source of the homemade spectroscopy setup is a commercial femtosecond amplifier laser system (35 fs, 1 kHz, 800nm, Spitfire Ace, Spectra Physics). The output pulse was split into two beams. The first beam was used to generate 400 nm laser pulses by second harmonic generation through a nonlinear optical crystal (α-BBO) which will act as the excitation pulses. The second beam with weaker energy was focused into a CaF_2 plate (4 mm thickness) to generate a white light continuum as the probe. The time delay between the pump beam and the probe pulses was controlled by a motorized delay stage. The transmitted probe light after sample was collected by a laser frequency synchronized fiber optical spectrometer (AvaSpec-ULS2048CL-EVO, Avantes). When chopping the pump laser beam with half of the laser frequency 1 kHz, the probe light in the case of pump on/off was acquired and finally the pump pulse induced optical density change of the sample was calculated. During the experiment, the pump intensity was set to be 7 uJ/cm^2. Elemental analysis data of samples were obtained using inductively coupled plasma atomic emission spectrometry (ICP-OES Varian 710-OES, USA). The electrochemical measurements were performed on a CHI660E electrochemical system (shanghai, China) using a standard three-electrode cell with a working electrode, a

platinum sheet (1 cm^2) counter electrode, and Ag/AgCl reference electrode. The working electrodes were prepared by the following step: Sample solutions dispersed in water/ethanol/Nafion (v:v = 800:160:40) with concentration of 2 mg/mL were prepared by sonication. The catalyst inks of the above solutions were then loaded onto a 1cm×2cm ITO glass electrode. Electrodes were exposed for 2 days to eliminate solvent and subsequently dried at 353 K for 1 day. For current-potential measurement, the electrolyte was 0.1 mol L^{-1} K_2SO_4 + 0.025 mol L^{-1} KH_2PO_4 + 0.025 mol L^{-1} Na_2HPO_4 solution, excitation light source was white LED lamp (100 W, $\lambda > 420$ nm). For Mott-Schottky (MS) measurement, the MS plots were carried out in 0.1 M KOH electrolyte at frequency of range from 100 to 1000 Hz. The flatband potential of the semiconductors was calculated by the Mott-Schottky relation:

$$\frac{1}{C^2} = \frac{2}{e\varepsilon\varepsilon_0 N_a} \times \left(-E + E_{fb} - \frac{KT}{e} \right)$$

Where C is the capacitance of the electrode, e is the elementary charge, ε is the dielectric constant of the electrode material, ε_0 is permittivity of vacumm, E is the applied potential, K is Boltzmann constant and T is the temperature. The potential of flatband is determined by the intercept of the potential axis, which obtained by fitting the liner to the plot. When $1/C^2$ is zero, the x-intercept is equal to flatband potential, and the dopant density N_a can be determined from the slope of the linear region.

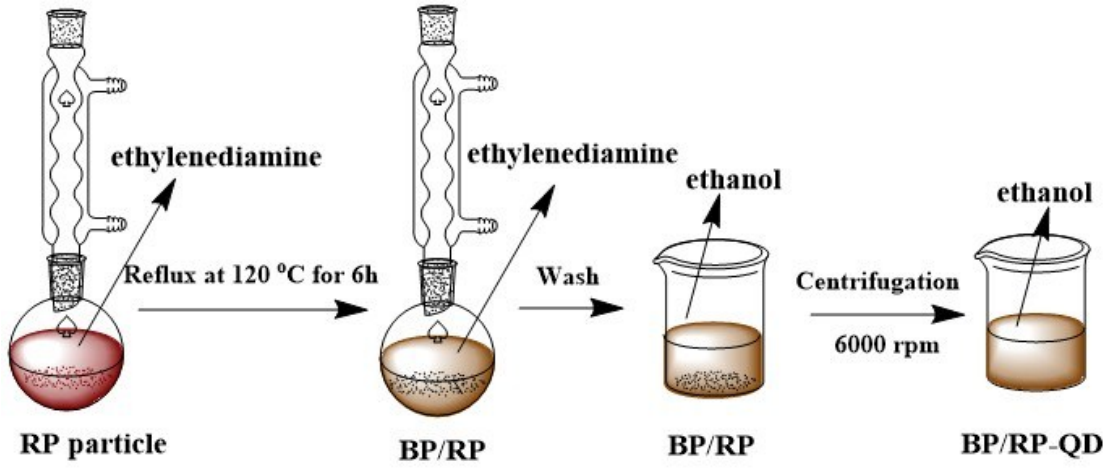

Scheme S1. Reaction route for synthesizing BP/RP-QD.

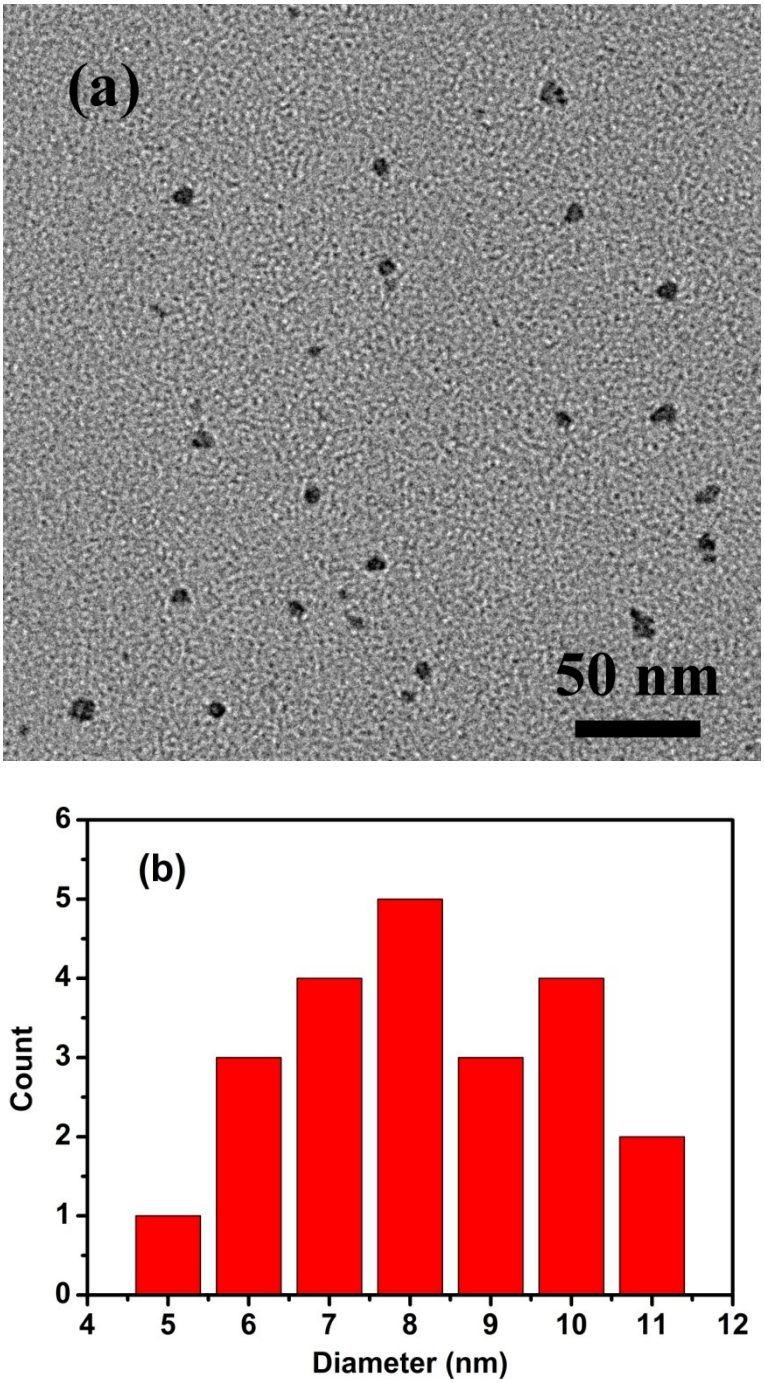

Fig. S1 (a) TEM image of RP-QD, (b) statistical analysis of sizes of 22 RP-QD measured from TEM image.

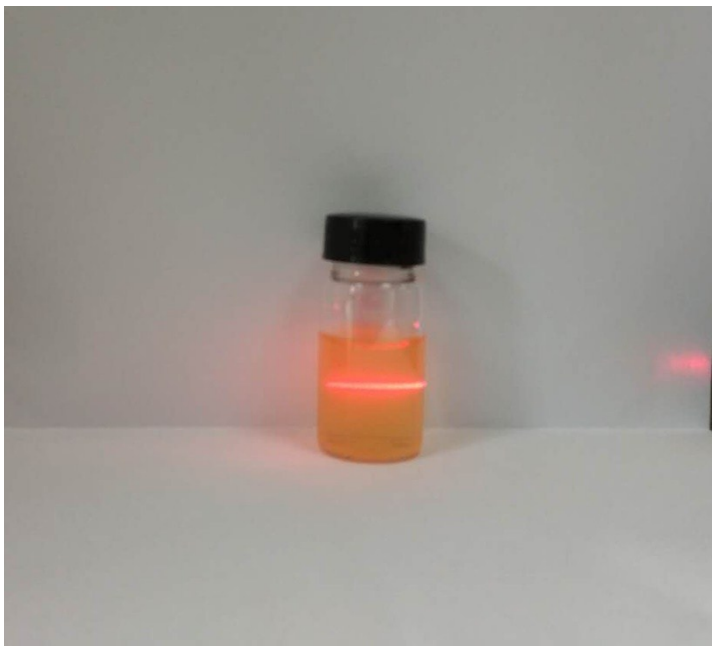

Fig. S2 Typical Tyndall effect of BP/RP-QD.

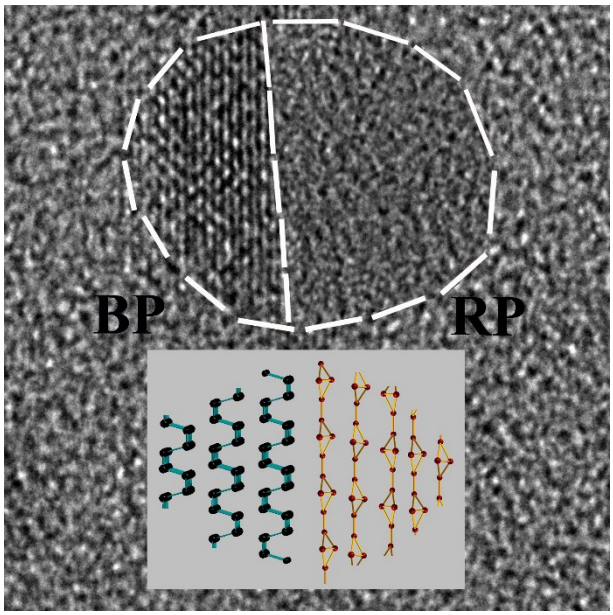

Fig. S3 The schematic structure of BP/RP-QD.

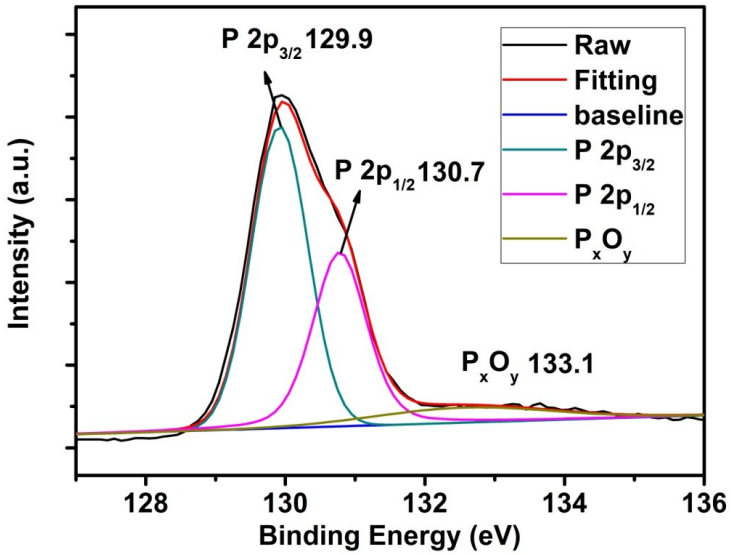

Fig. S4 XPS spectra of P 2p of BP/RP-QD.

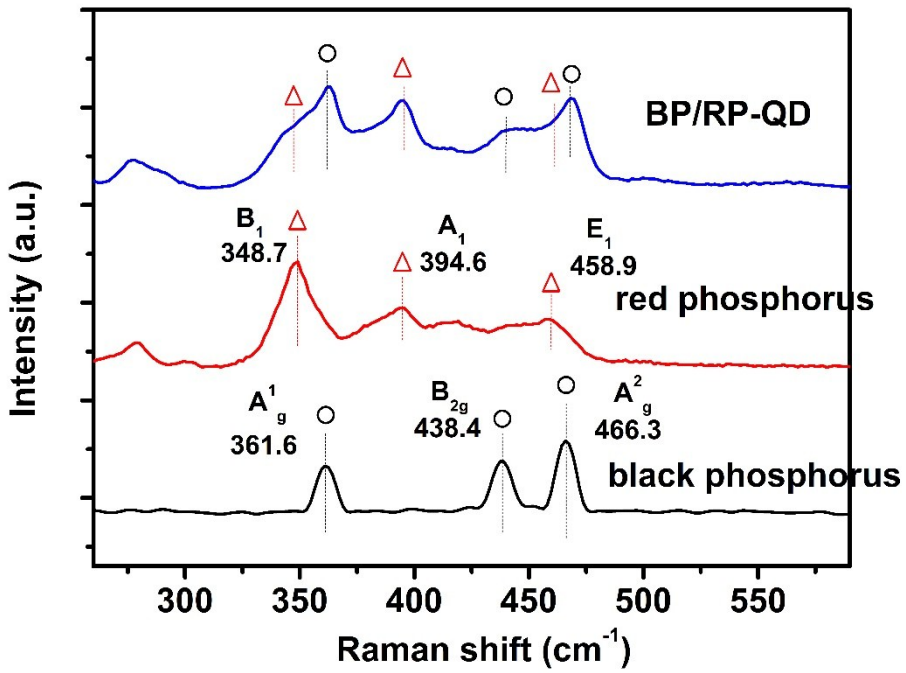

Fig. S5 Raman spectra of black phosphorus, red phosphorus and BP/RP-QD. Black circles and red triangles represent the peak positions of black phosphorus and red phosphorus, respectively.

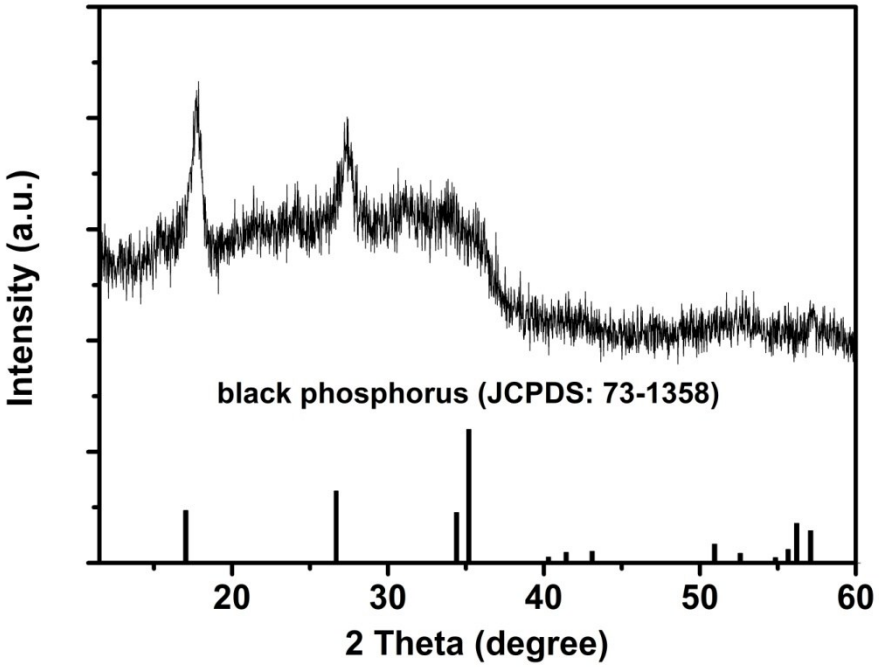

Fig. S6 XRD pattern of BP/RP-QD.

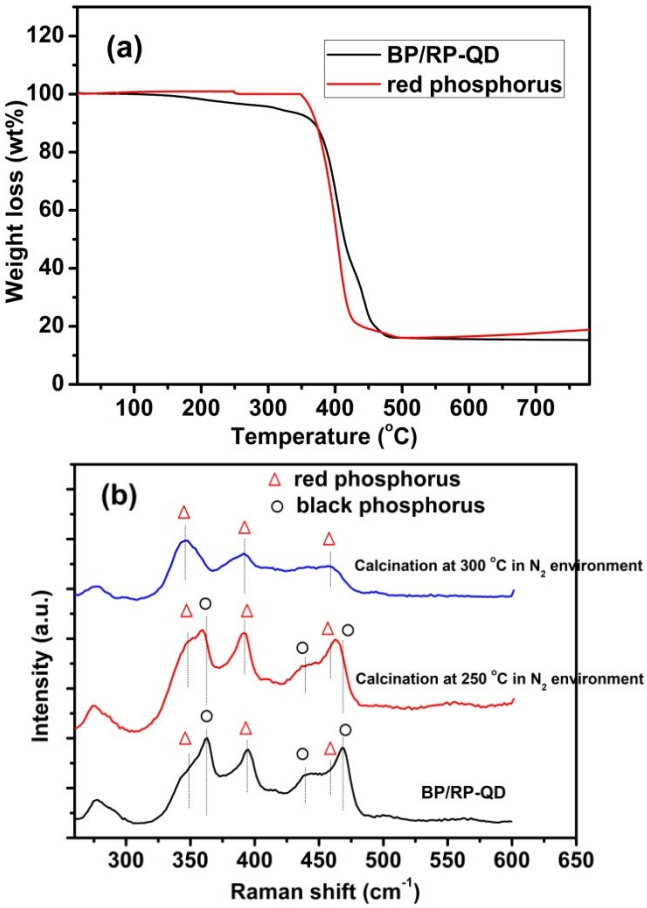

Fig. S7 (a) TGA curves of BP/RP-QD and red phosphorus under N_2 environment with a heating rate of 3 $^{o}C \cdot min^{-1}$, (b) Raman spectra of BP/RP-QD calcinated at 250 and 300 ^{o}C for 1 h under N_2 environment, Black circles and red triangles represent the peak positions of black phosphorus and red phosphorus, respectively.

TGA was carried out under N_2 environment to estimate the content of black phosphorus in BP/RP-QD (Fig. S6a). It can be seen that BP/RP-QD has about 7~8 % weight loss in the first weight-loss step (<360 ^{o}C). After the temperature is heated to 360 ^{o}C, red phosphorus begins to sublimate. We speculate that weight loss in the first step is attributed to the sublimation of black phosphorus. In order to confirm our point of view, phase compositions of BP/RP-QD calcinated at different temperature under N_2 environment were tested by Raman spectra (Fig. S6b). It can be seen that black phosphorus completely disappeared in BP/RP-QD when the temperature is raised to 300 ^{o}C. Therefore, it is reasonable to infer that 7~8 % weight loss in TGA is attributed to the sublimation of black phosphorus.

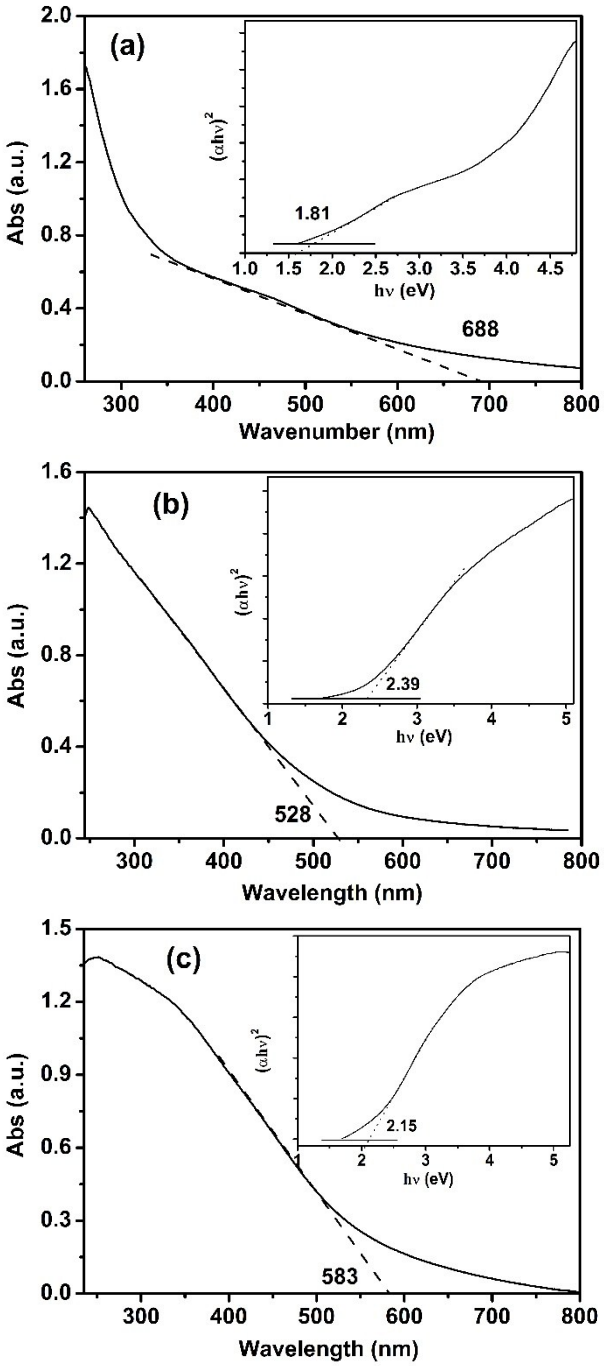

Fig. S8. UV-vis absorption spectra of (a) BP-QD, (b) RP-QD, (c) BP/RP-QD in NMP, inset: plot of $(\alpha h\nu)^2$ versus the energy of the exciting light ($h\nu$) curve. Black phosphorus and red phosphorus are both direct bandgap materials,[S2] thus r=2 for Tauc plot $(\alpha h\nu)^r$ versus $h\nu$.

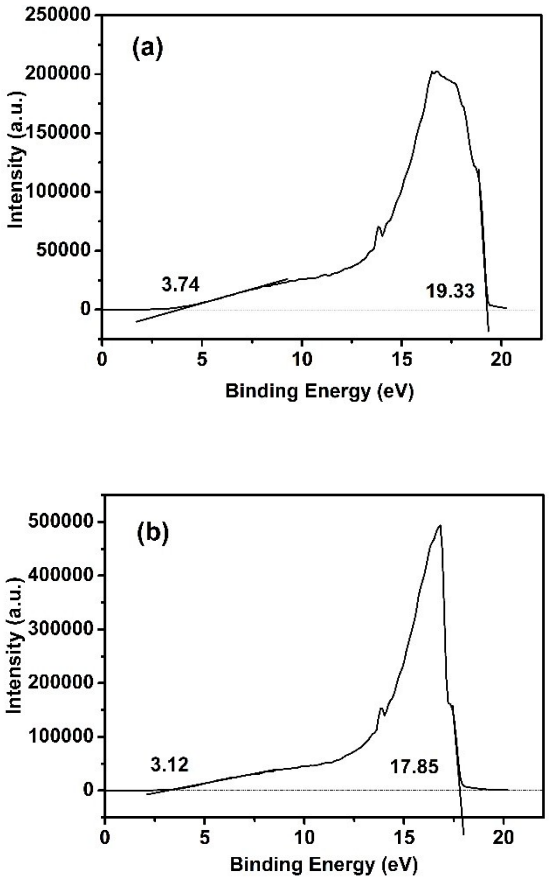

Fig. S9 UPS spectra of (a) BP-QD and (b) RP-QD.

The valence band level (E_{VB}) is calculated by subtracting the width of UPS spectra from the He Ⅰ excitation energy (21.22 eV).[S3, S4] Based on the Fig. S9a and S9b, E_{VB} of BP-QD and RP-QD were calculated to be -5.63 and -6.49 eV versus vacuum level, respectively. On the basis of the relationship between vacuum level in electron volts and RHE in volts, where -4.44 eV versus vacuum level is equal to 0 V versus RHE,[S4-S6] E_{VB} of BP-QD and RP-QD can also be converted to 1.19 and 2.05 V versus RHE, respectively.

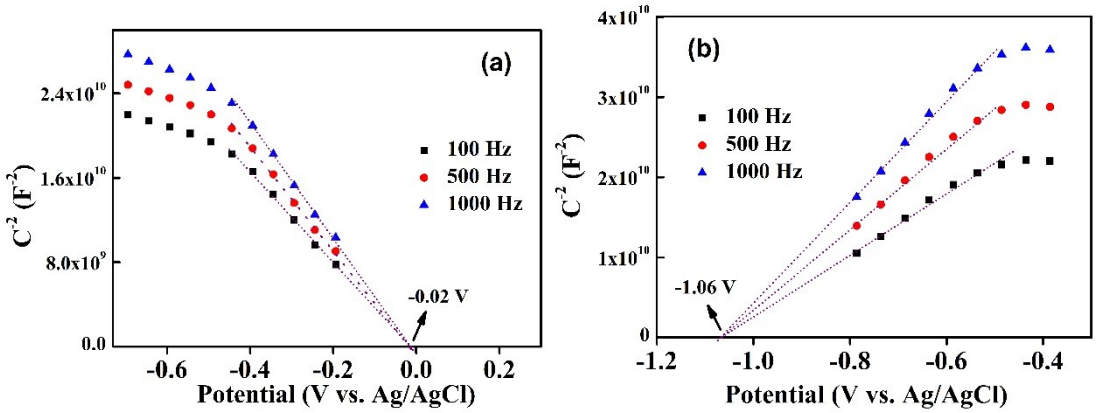

Fig. S10 Mott-Schottky plots of (a) BP-QD and (b) RP-QD.

As shown in Fig. S10a, the Mott-Schottky plots demonstrated that BP-QD with a negative slope represents the p-type semiconductor and its flatband potential was -0.02 V (versus Ag/AgCl) corresponding to 0.95 V (versus RHE). Generally, the potential measured against Ag/AgCl reference can be converted into RHE potential by the follow equation.[S7-S9]

$$E(versus\ RHE) = E(versus\ Ag/AgCl) + E_0 + 0.0591pH$$

The measured pH value of electrolyte is about 13, and E_0 = 0.1976 V. Therefore, the calculated flatband position of BP-QD is 0.95 V versus RHE. While RP-QD with a positive slope represents the n-type semiconductor, and its flatband potential was -1.06 V (versus Ag/AgCl) corresponding to -0.09 V (versus RHE) (Fig. S10b). Supposing that valence band potential (VBM) of p-type semiconductor or conduction band potential (CBM) of n-type semiconductor has differences of 0.2 V to their respective flatband potential,[S10-S12] the VBM of BP-QD and CBM of RP-QD was estimated to be 1.15 and -0.29 V (versus RHE), respectively. Furthemore, CBM of BP-QD and VBM of RP-QD can be calculated to be -0.66 and 2.10 V (versus RHE), respectively, using their band gaps. The band potentials obtained from M-S plots are similar to the results of UPS spectra.

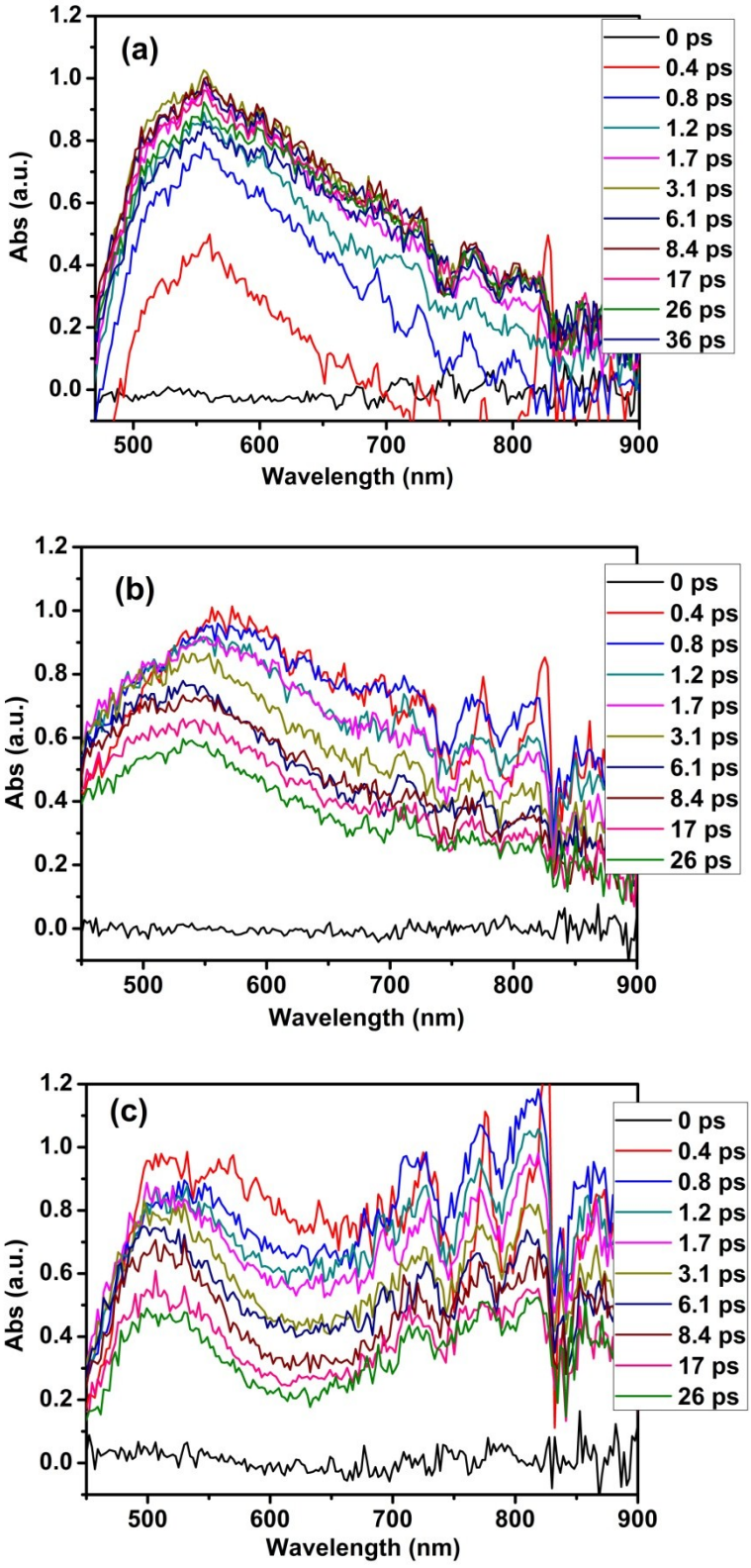

Fig. S11 TAS spectra for BP-QD, RP-QD and BP/RP-QD after irradiation under 400 nm.

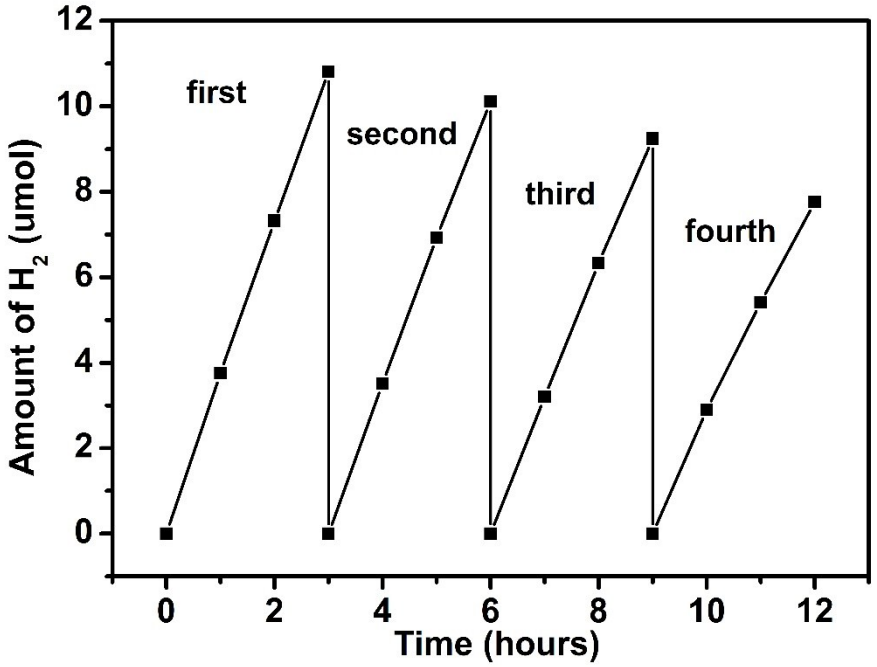

Fig. S12 Photocatalytic durability test for 2 wt% Co-BP/RP-QD.

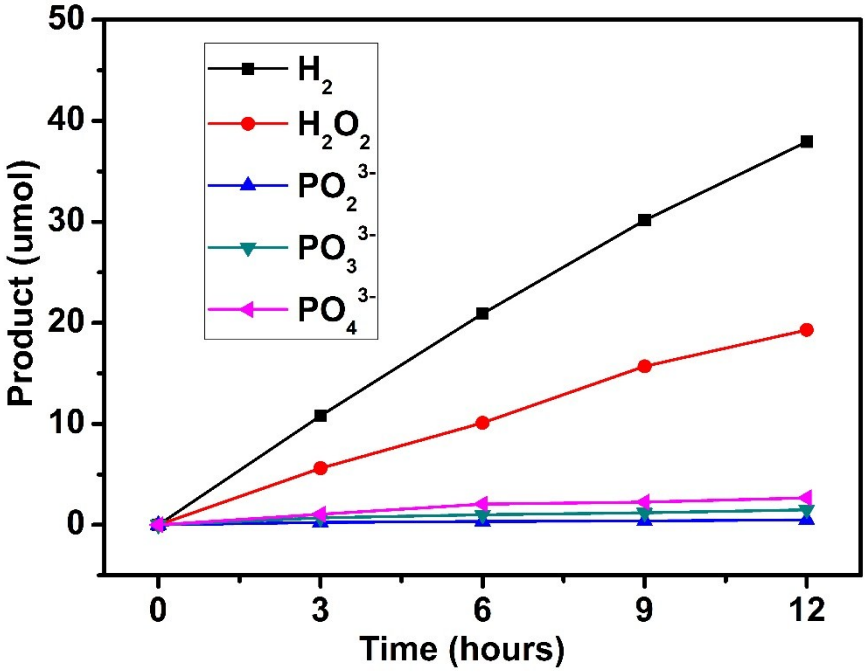

Fig. S13 Total amount of reduction and oxidation products generated during the durability test.

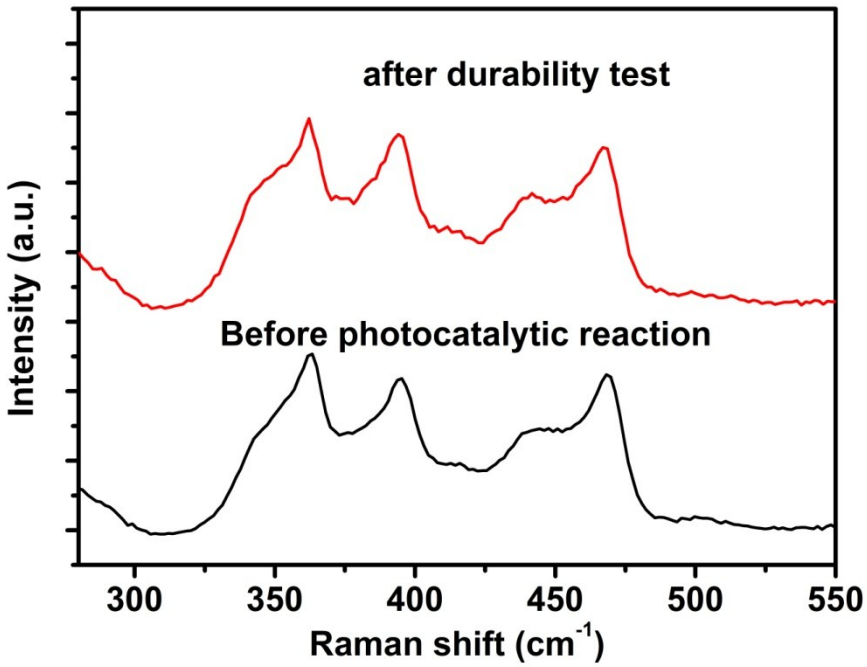

Fig. S14 Raman spectra of 2 wt% Co-BP/RP-QD before and after photocatalytic durability test.

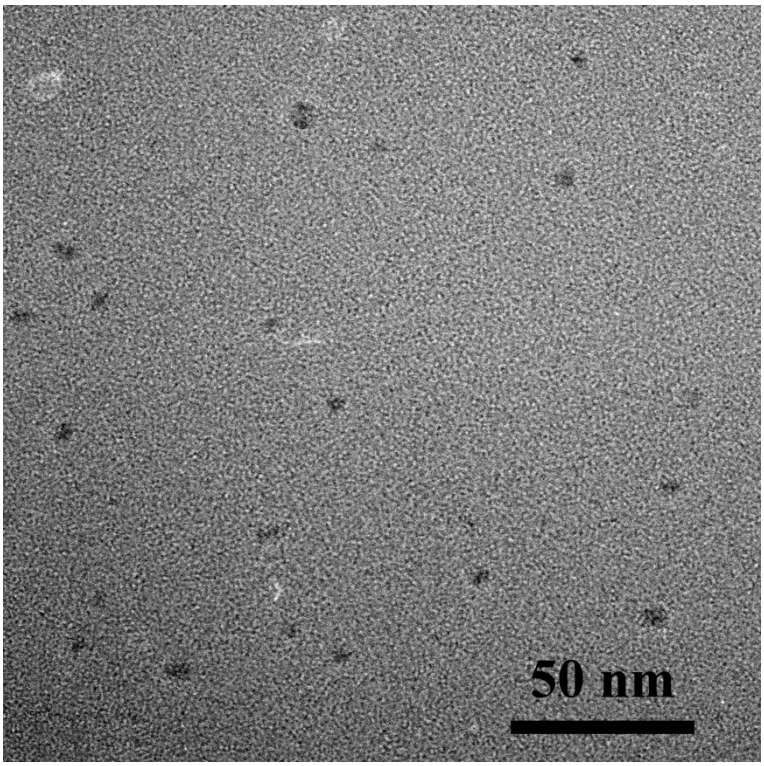

Fig. S15 TEM image of 2 wt% Co-BP/RP-QD after photocatalytic durability test.

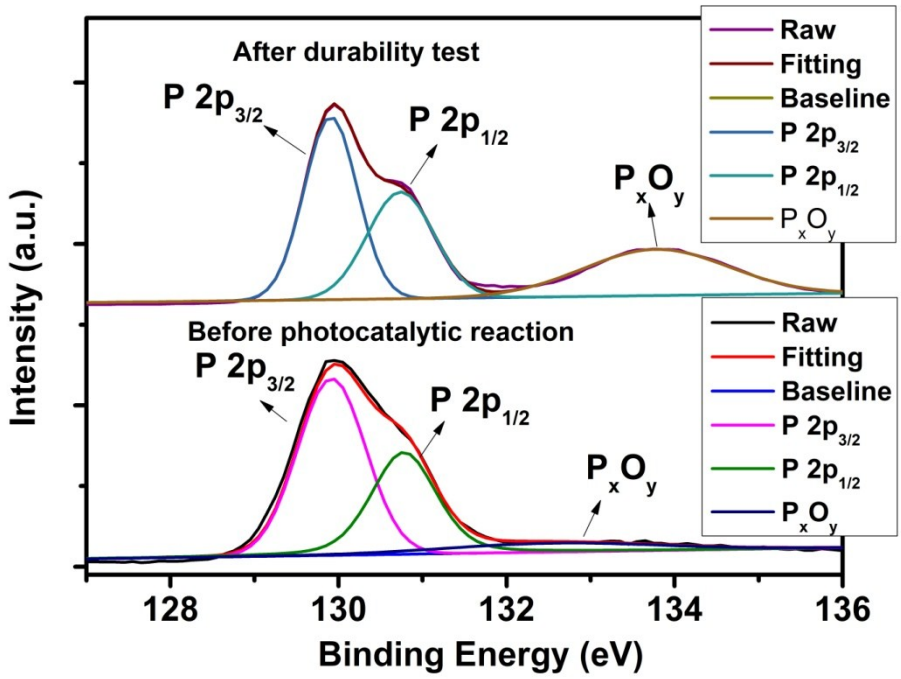

Fig. S16 XPS spectra of P 2p of 2 wt% Co-BP/RP-QD before and after photocatalytic durability test.

Table S1. The band gaps of black phosphorus with different layer numbers.

Thickness (layers)	**1**	**2**	**3**	**4**	**Bulk**	**Refs**
Band gap (eV)	2.15	1.70	1.48	1.36	1.08	Ref [6a]
	2.0	1.30	1.06		0.30	Ref [6b]
	1.94	1.70	1.3	0.8	0.43	Ref [6c]
	1.60	1.01	0.68	0.46	0.1	Ref [6d]
	1.52	1.01	0.79	0.67	0.36	Ref [6e]
		1.02	0.79	0.68		Ref [6f]

Notes and references.

(S1) X. Zhang, H. M. Xie, Z. D. Liu, C. L. Tan, Z. M. Luo, H. Li, J. D. Lin, L Q. Sun, W. Chen, Z. C. Xu, L. H. Xie, W. Huang, H. Zhang, *Angew. Chem. Int. Ed*., 2015, 54, 3653-3657.

(S2) Z. Hu, L. Yuan, Z. Liu, Z. Shen, J. C. Yu, *Angew. Chem. Int. Ed.,* 2016, 55, 9580-9585.

(S3) L. Wang, Y. Y. Wan, Y. J. Ding, S. K. Wu, Y. Zhang, X. L. Zhang, G. Q. Zhang, Y. J. Xiong, X. J. Wu, J. L. Yang, H. X. Xu, *Adv. Mater.,* 2017, 29, 1702428.

(S4) M. S. Zhu, S. Kim, L. Mao, M. Fujitsuka, J. Y. Zhang, X. C. Wang, T. Majima, *J. Am. Chem. Soc.,* 2017, 139, 13234-13242.

(S5) J. Liu, Y. Liu, N. Liu, Y. Han, X. Zhang, H. Huang, Y. Lifshitz, S. T. Lee, J. Zhong, Z. Kang, Science, 2015, 347, 971-975.

(S6) J. D. Hu, D. Y. Chen, Z. Mo, N. J. Li, Q. F. Xu, H. Li, J. H. He, H. Xu, J. M. Lu, *Angew. Chem. Int. Ed*., 2019, 58, 2073-2077.

(S7) M. S. Zhu, X. Y. Cai, M. Fujitsuka, J. Y. Zhang, T. Majima, *Angew. Chem. Int. Ed*. 2017, 56, 2064-2068;

(S8) M. S. Zhu, Z. C. Sun, M. Fujitsuka, T. Majima, *Angew. Chem. Int. Ed*, 2018, 57, 2160-2164;

(S9) B. Tian, B. Tian, B. Smith, M. C. Scott, Q. Lei, R. N. Hua, Y. Tian, Y. Liu, *Proc. Natl. Acad. Sci. USA,* 2018, **115**, 4345-4350.

(S10) K. He, T. T. Tsega, X. Liu, J. T. Zai, X. H. Li, X. J. Liu, W. H. Li, N. Ali, X. F. Qian, Angew. Chem. Int. Ed., 2019, 58, 11903-11909.

(S11) D. Liu, J. Wang, X. J. Bai, R. L. Zong, Y. F. Zhu, Adv. Mater., 2016, 28, 7284-7290.

(S12) M. Xu, T. Ye, F. Dai, J. Yang, J. Shen, Q. He, W. Chen, N. Liang, J. Zai, X. Qian, ChemSusChem, 2015, 8, 1218-1225.